

Solution-Processed Self-Powered Transparent Ultraviolet Photodetectors with Ultrafast Response Speed for High-Performance Communication System

Huajing Fang, Cheng Zheng, Liangliang Wu, Yi Li, Jian Cai, Mingxiang Hu, Xiaosheng Fang,* Rong Ma, Qing Wang, and Hong Wang*

Transparent ultraviolet (UV) photodetectors are an essential component of next-generation “see-through” electronics. However, the current photodetectors often suffer from relatively slow response speeds and high driving voltages. Here, all-solution-processed UV photodetectors are reported that are facilely prepared from environmentally friendly and abundant materials. The UV photodetectors are composed of a titanium dioxide thin film as the photosensitive layer sandwiched between two different transparent electrodes to form asymmetric Schottky junctions. The photodetector with high optical transparency can operate at zero bias because of spontaneous separation of photogenerated electron–hole pairs by the built-in electric field. The resulting self-powered photodetector displays high sensitivity to broadband UV light (200–400 nm). In particular, an ultrafast response speed up to 44 ns is obtained, representing a significant improvement over those of the conventional transparent photodetectors. Moreover, the photodetector has been successfully applied, for the first time, in a UV communication system as the self-powered signal receiver. This work uniquely combines the features of high optical transparency and self-power ability into UV photodetectors and would enable a broad range of optoelectronic applications.

transparent electronics include organic light emitting diodes,^[6] thin film field effect transistor (FET),^[7] supercapacitors,^[8] solar cells,^[9] nanogenerators,^[10] and memory.^[11] Ultraviolet (UV) photodetector with the ability of converting UV light into electrical signal is crucial for optoelectronic systems, e.g., function as a signal receiver in UV communication systems.^[12–14] Different from other wireless communication methods, UV communication systems are suitable for radio silent condition, with intrinsic advantages of non-line-of-sight communication, anti-interference, and anti-interception.^[15,16] In particular, transparent UV photodetectors would realize the “see-through” receiver, which is irreplaceable in smart windows and many other special applications. With the steadily increased demands, the transparent UV photodetector has become a key research issue in the past few years. For example, Tian et al. fabricated a fully transparent photodetector with a high

1. Introduction

Transparent electronics with both excellent performance and high transparency are emerging technologies for next-generation “see-through” functional devices.^[1–5] The most recently developed

photodark current ratio of 4600 based on the electrospun ZnO–SnO₂ heterojunction nanofibers.^[17] With a unique Ω -shaped core–shell nanostructure, Hu et al. reported a ZnO–SnO₂ based photodetector with enhanced responsivity of $\approx 100 \text{ A W}^{-1}$.^[18] However, the current transparent photodetectors with a lateral


Dr. H. J. Fang
State Key Laboratory for Mechanical Behavior of Materials
School of Material Science and Engineering
Xi'an Jiaotong University
Xi'an 710049, China

C. Zheng, L. L. Wu, Y. Li, R. Ma, Prof. H. Wang
School of Electronic and Information Engineering
and State Key Laboratory for Mechanical
Behavior of Materials
Xi'an Jiaotong University
Xi'an 710049, China

J. Cai, M. X. Hu, Prof. X. S. Fang
Department of Materials Science
Fudan University
Shanghai 200433, China
E-mail: xshfang@fudan.edu.cn

Prof. Q. Wang
Department of Materials Science and Engineering
The Pennsylvania State University
University Park
PA 16802, USA

Prof. H. Wang
Department of Materials Science and Engineering
& Shenzhen Engineering Research Center for Novel
Electronic Information Materials and Devices
Southern University of Science and Technology
Shenzhen 518055, China
E-mail: wangh6@sustc.edu.cn

 The ORCID identification number(s) for the author(s) of this article can be found under <https://doi.org/10.1002/adfm.201809013>.

DOI: 10.1002/adfm.201809013

architecture often suffer from high driving voltages (more than 5 V) and relatively slow response speeds (i.e., seconds) due to large electrode spacing. Changing the device into a longitudinal structure can effectively reduce the electrode spacing, which mainly depends on the thickness of the photosensitive layer. Patel et al. prepared a high-quality p-NiO/n-ZnO heterojunction by sputtering.^[19] With 5 V bias, this all transparent metal oxide device exhibited a fast photoresponse time of 24 ms. Yet it remains challenging to determine efficient device structures with faster response speeds as well as low manufacturing cost.

Meanwhile, the continued development of electronics toward miniaturization and portability necessitates independent and sustainable operations of devices. It is thus highly desirable to develop the self-powered microsystem/nanosystem capable of operating without external power sources (e.g., batteries).^[20,21] Harvesting the renewable energy from environment is an effective solution. Various energy harvesting technologies have been reported in recent years, such as photovoltaics for the energy from light,^[22,23] nanogenerators for the mechanical energy,^[24] and thermoelectric generator for the energy from heat.^[25] Construction of the built-in electric field by Schottky or p–n junctions has been a widely adopted approach to self-powered UV photodetectors.^[26–28] When UV light irradiates on the photodetectors, the photogenerated electron–hole (e–h) pairs are separated in line with the energy level alignment at the interfaces. However, many of the junction-based photodetectors require vacuum processing techniques, which are relatively complicated and expensive. Moreover, it remains challenging to achieve simultaneously high optical transparency and

self-powered ability in UV photodetectors due to the limited material selection for building blocks of transparent junctions.

Compared with vacuum processing techniques, solution processing is a promising alternative with advantages of simple, low-cost, and easy to mass produce. In this work, we demonstrate a solution-processed self-powered UV photodetector with $\approx 70\%$ optical transparency in visible range. By stacking a titanium dioxide (TiO₂) film with two different transparent electrodes, asymmetric Schottky junctions are formed back to back in the device. At zero bias condition, the devices exhibit a high responsivity of 32.5 mA W⁻¹ as well as a broadband response (200–400 nm). More notably, an ultrafast response speed of 44 ns has been achieved in the self-powered photodetector. The resulting transparent UV photodetector with asymmetric Schottky junctions opens new avenue for next-generation “see-through” functional devices.

2. Results and Discussion

Semiconductor materials are essential in photodetectors for the generation of electron–hole pairs through absorption of incident photons. TiO₂ is one of the most important and widely investigated semiconductors with high chemical stability and nontoxic properties.^[29] Because of its wide bandgap (3.2 eV, anatase; 3.0 eV, rutile) and superior electron transport properties, it has been used as a sensitive material in the selective UV wavelength ranges.^[30,31] Herein, the TiO₂ thin films were synthesized by a sol–gel method. Details can be found in the Experimental Section. As shown in Figure 1a, the prepared precursor shows

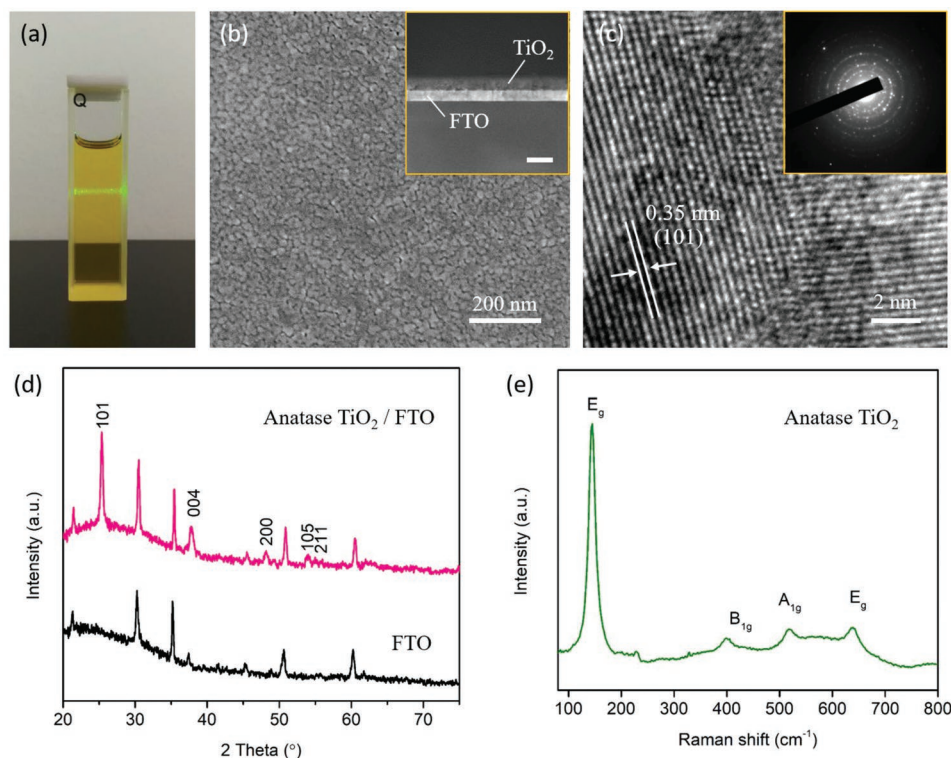


Figure 1. a) Digital photograph of the TiO₂ colloidal precursor, Tyndall effect was visible when irradiated with a green laser beam. b) SEM image of the annealed TiO₂ film. Inset is a cross-sectional SEM image of TiO₂ film on FTO substrate, the scale bar is 400 nm. c) HRTEM image of TiO₂ film and inset show the SAED pattern. d) XRD patterns of the FTO substrate and annealed TiO₂ film. e) Raman spectrum of annealed TiO₂ film upon excitation at 532 nm.

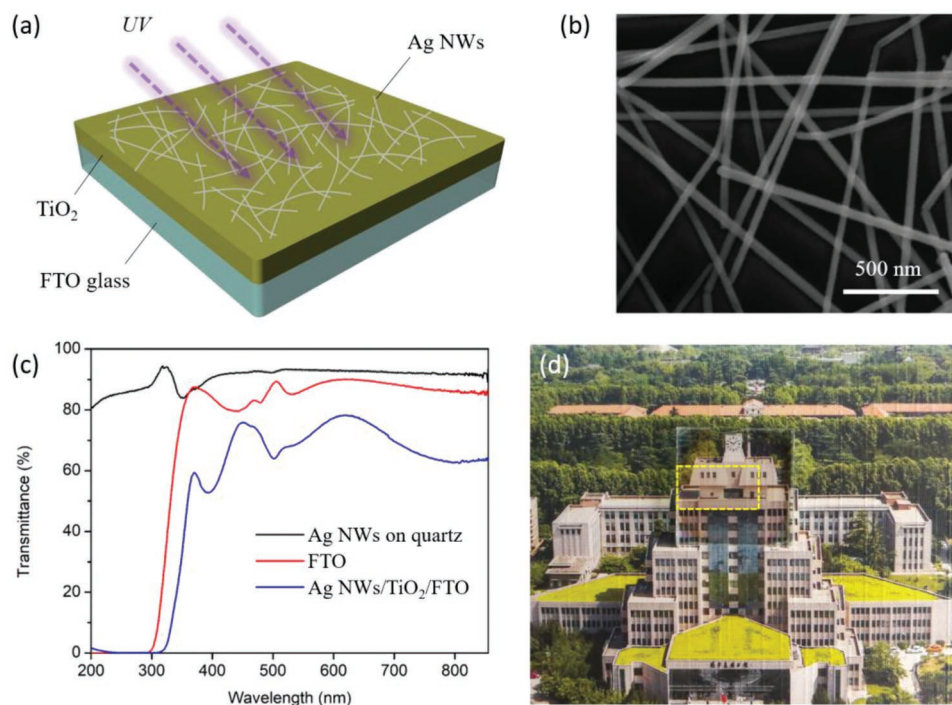


Figure 2. a) Schematic illustration of the transparent UV photodetector. b) SEM image of Ag NWs top electrode. c) Transmittance spectrum of the FTO glass, Ag NWs, and total device. d) Digital image of the transparent UV photodetector, the area covered with Ag NWs network is denoted with a yellow dotted line.

light-yellow color. Upon exposure to a green laser beam, the obvious Tyndall scattering effect suggests the presence of colloids. A uniform thin film was formed by spin-coating. The surface morphology as seen from the scanning electron microscopic (SEM) image (Figure 1b) shows a compact and uniformly interconnected TiO_2 nanocrystalline structure. As shown in the inset of Figure 1b, a flat TiO_2 layer was deposited on the fluorine doped tin oxide (FTO) substrate with a thickness of 200 nm. The high resolution transmission electron microscopy (HRTEM) of TiO_2 film is depicted in Figure 1c, in which the lattice fringes with a spacing of 0.35 nm can be clearly observed, corresponding to the (101) planes of anatase TiO_2 . Inset shows the selected area electron diffraction (SAED) pattern, with the typical diffraction rings of polycrystalline. The crystal structure of the TiO_2 layer was characterized by X-ray diffraction (XRD). Figure 1d shows the XRD pattern of a sample annealed at 550 °C. In addition to the diffraction peaks of FTO substrate, all the other peaks correspond to the anatase phase TiO_2 .^[32] The average crystal size of 24 nm corresponding to the (101) peak was calculated by Scherrer formula.^[33] It is obvious that the film has a pure anatase phase and no impurity phase such as rutile phase is formed during the annealing process. Notably, anatase TiO_2 was selected due to the better carrier transport capability and a lower annealing temperature.^[34] Raman spectroscopy was employed to further study the microstructure of the annealed sample because Raman scattering is very sensitive to the local crystallinity. The TiO_2 film displays four peaks corresponding to the Raman active fundamental modes for anatase phase, as shown in Figure 1e. The E_g peaks at 144 and 637 cm^{-1} are mainly caused by the symmetric stretching

vibration of O–Ti–O bond. The B_{1g} peak at 398 cm^{-1} corresponds to the symmetric bending vibration of O–Ti–O bond, and the A_{1g} peak at 517 cm^{-1} is attributed to the antisymmetric bending vibration of O–Ti–O bond.^[35,36] The Raman spectrum is consistent with the XRD pattern, in which no other phases like rutile were detected. These results demonstrate that a high-quality TiO_2 film can be fabricated by sol–gel method, which is the prerequisite for high performance optoelectronic device.

Figure 2a shows the schematic of device architecture of the designed UV photodetector, in which the TiO_2 thin film is located between the two electrodes to form a sandwich structure. Such a design not only shortens the electrode spacing significantly, but also ensures the photogenerated carriers separate along the built-in electric field, maximizing the effect of Schottky junctions. To form a fully transparent device, silver nanowires (Ag NWs) were used as the top electrode, which were fabricated by directly drop casting Ag NWs dispersion on the surface of TiO_2 thin film. After drying, the Ag NWs spontaneously formed continuous and random networks. Figure 2b presents an SEM image of the electrode, showing that the networks are mostly composed of individual nanowires with a diameter of ≈ 30 nm. Moreover, the good contact at the junction of nanowires ensures a convenient electronic transport between different nanowires. Consequently, the Ag NWs electrode shows a low sheet resistance of 35 ohm sq^{-1} . The transmittance spectrum of the Ag NWs transparent electrode is shown in Figure 2c, compared with that of traditional FTO electrodes. Although both electrodes show a high transmittance of above 80% in the visible and near-infrared region, there is a significant difference in the UV region. While Ag NWs

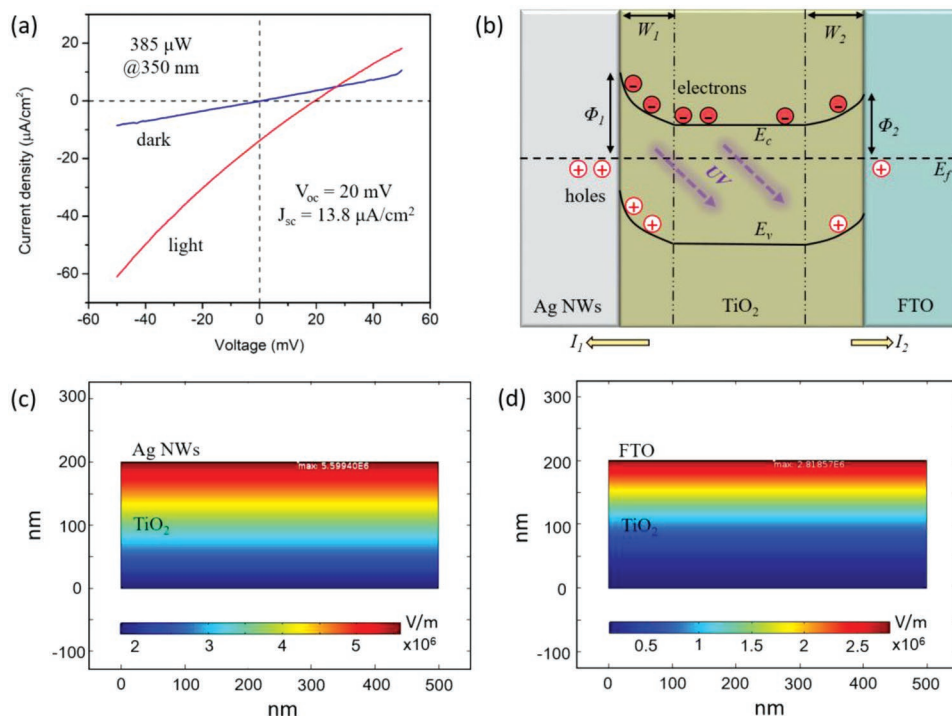


Figure 3. a) J – V curves of the photodetector in the dark and under illumination of 350 nm UV light. b) Energy band diagram of the asymmetric Schottky junction-based photodetector under UV illumination. c) The electric field distribution at $\text{TiO}_2/\text{Ag NWs}$ junction. d) The electric field distribution at TiO_2/FTO junction.

electrode maintains high light transmission, the transmittance spectrum of FTO electrode shows a sharp drop around 350 nm owing to the absorption of UV by FTO layer and glass substrate. As shown in Figure 2c, the average transmittance of the Ag NWs/ TiO_2 /FTO device in the visible range T_{avg} is $>70\%$, which satisfies the requirement of transparent electronics.^[37] The photograph of the device shown in Figure 2d further confirms its transparency.

To investigate the photoelectric properties of the prepared transparent device, the current density versus bias voltage (J – V) characteristics were measured at room temperature. As can be seen in Figure 3a, the J – V curve under dark condition passes through the origin without any noticeable rectification effect, indicative of the formation of a back to back Schottky diode in the sandwiched structure.^[38] Under the 350 nm UV illumination, the J – V curve exhibits a down shift due to the photogenerated carriers. The short-circuit current density (J_{sc}) increases to $13.8 \mu\text{A cm}^{-2}$, and the open-circuit voltage (V_{oc}) reaches to 20 mV based on the photovoltaic effect. The transport direction of photogenerated carriers is critical to determining the junctions inside the device. Comparing the output current polarity with other power supplies (see Figure S1, Supporting Information), it is found that the net holes inside the device move toward the Ag NWs, and the net electrons are injected into the FTO. Hence, there must exist a Schottky junction at the $\text{TiO}_2/\text{Ag NWs}$ interface. To clarify the Schottky contact between TiO_2 and FTO, I – V curves and transient photoresponse of a FTO/ TiO_2 /FTO configuration were measured. As shown in Figure S2 (Supporting Information), the typical nonlinear relationship of the dark I – V curve confirms the Schottky junction of the $\text{TiO}_2/$

FTO interface. To fully understand the mechanism of the transparent photodetector, a physical model is proposed based on the energy band theory. The electron affinity of TiO_2 (4.0 eV) is lower than the work function of FTO (4.4 eV).^[39] The work function of pure Ag NWs is reported to be 4.57 eV,^[33] however, it may significantly increase to 4.9–5.0 eV with slight oxidation.^[40] As illustrated in Figure 3b, two asymmetric Schottky junctions were formed back to back at the interfaces between TiO_2 and electrodes. When the TiO_2 film was illuminated with UV light, photogenerated e–h pairs can be separated by the built-in electric field at the Schottky barriers interfaces. Since the Schottky barriers height of $\text{TiO}_2/\text{Ag NWs}$ ($\Phi_1 = 0.9 \text{ eV}$) is larger than that of TiO_2/FTO ($\Phi_2 = 0.4 \text{ eV}$), the left side ($\text{TiO}_2/\text{Ag NWs}$) has more efficient separation, leading to a larger current ($I_1 > I_2$). As a result, the total current direction of the device is determined by I_1 . Finite element analysis (COMSOL Multiphysics) has been carried out to further understand the difference between these two Schottky barrier interfaces. All the required parameters of device simulation are listed in Table S1 (Supporting Information). Figure 3c,d shows the 2D model of the $\text{TiO}_2/\text{Ag NWs}$ and TiO_2/FTO Schottky junctions, respectively. The thickness of TiO_2 layer was set to 200 nm and the electrode is located at the upper side of the TiO_2 film. The calculation of the spatial distribution of the electric field shows that the electric field presents a streaks characteristic in both cases. Different colors in the model vividly describe the relative strength of the electric field. Obviously, the field strength at the interface between the TiO_2 film and electrode reaches the highest value and gradually decreases as the distance increases. Therefore, both interfaces can respond to the UV illumination and provide the

photogenerated current under self-biased condition. By carefully comparing the two junctions, it is found that the electric field formed by TiO₂/Ag NWs is significantly stronger than that of TiO₂/FTO. We further calculated the spatial distribution of the electric field in Ag NWs/TiO₂/FTO structure (see Figure S3, Supporting Information), it also shows that the field strength near the TiO₂/Ag NWs interface is higher. Hence, TiO₂/Ag NWs junction has much more efficient separation of photogenerated e–h pairs under UV illumination, consistent with our experimental data. All these results indicate that the combination of Ag NWs and FTO as opposite electrodes is an effective design scheme for transparent Schottky devices.

Since the asymmetrical Schottky barriers provide the driving force to separate the photogenerated carriers, the resulting device can work as a self-powered photodetector. The switching behaviors at zero bias were measured under different light intensities. As shown in Figure 4a, the device can generate a periodically changing current under intermittent

illumination. The photocurrent (defined as the current difference between the light and dark state, $I_{ph} = I_l - I_d$) increases with the light intensity, consistent with the fact that the concentration of photogenerated carriers is positively correlated to the absorbed photon flux.^[17] Inset is a magnified image of $I-t$ curve under 0.4 μW illumination, in which a distinct switching behavior with 13 nA photocurrent can be observed. The photocurrent increases to 1.72 μA (steady state) when the incident light intensity reaches to 385 μW , with a high photodark current ratio of around 1700. It should be noted that the current signal shows sharp positive spikes and tiny negative spikes, especially when the light intensity is stronger than 8.7 μW . The appearance of spikes is very common in the TiO₂ based optoelectronic devices, which is caused by the initial electron–hole pair separation in the depletion layer and/or the local capacitance effects.^[41–43] In fact, the Ag NWs/TiO₂/FTO device can also be regarded as a capacitor with a thickness of 200 nm. Its capacitance may be affected by the light (or the

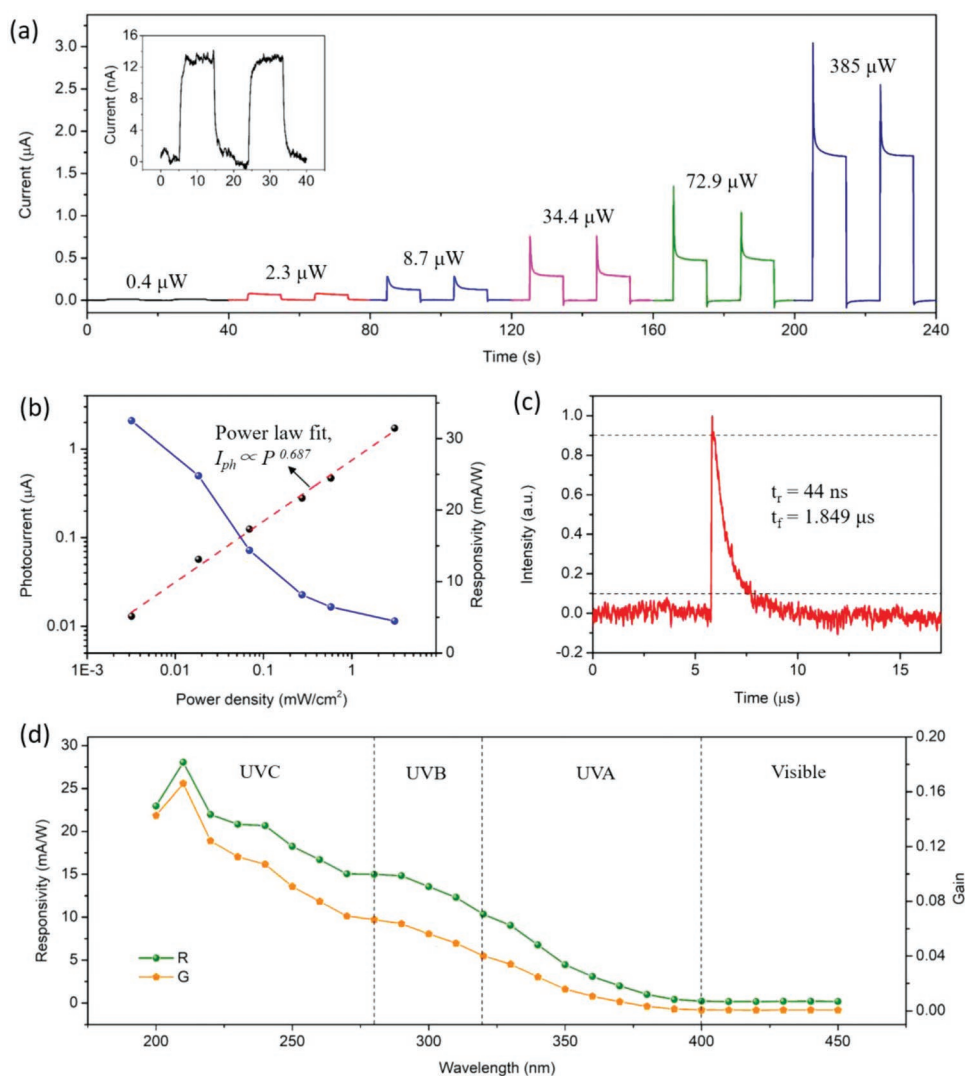


Figure 4. a) Photoswitching behaviors of the self-powered photodetector under different light intensity. Inset is a magnified image of $I-t$ curve under 0.4 μW illumination. b) Photocurrent and responsivity as a function of power density at 350 nm. c) Single period of pulse response measured at 0 V bias. d) Spectral photoresponse and gain of the self-powered photodetector.

heat generated by incident light). Therefore, periodic illumination will result in a fast charge and discharge cycle. The current generated during charging and discharging process is reversed, so there exist spikes in both the rise and fall time-dependent photoresponse. The amount of transferred charge during charging and discharging process should be equal, but the positive spikes are much larger than negative ones. This implies that the initial e–h pair separation in the depletion layer plays a more significant role in generating positive spikes upon UV illumination. Such a positive spike current will decay to a constant value until the generation and recombination of e–h pairs achieve an equilibration. Therefore, a lower steady state photocurrent has been obtained. The quantitative dependence of the steady state photocurrent on the light power density is plotted in Figure 4b, which can be well fitted to a power law, as shown in Equation (1)

$$I_{\text{ph}} \propto P^{\beta} \quad (1)$$

Here, P is the light power density and β is a factor that determines the response of the photocurrent to power density. The fitting can give a linear behavior, in which β is found to be 0.687. Such a nonunity exponent ($0.5 < \beta < 1$) suggests a complex process in the transparent devices, including the generation, separation, recombination, and trapping of electron–hole pairs.^[44] Normally, responsivity (R) is a key evaluation parameter for photodetectors, and can be expressed as the following Equation (2)^[44]

$$R = I_{\text{ph}} / (P \cdot S) \quad (2)$$

where I_{ph} is the photocurrent, P is the light power density, and S is the effective illumination area. The R values with various light power density were calculated and summarized in Figure 4b. It is clear that R decreases with the increase of power density. At the power density of $3.18 \mu\text{W cm}^{-2}$, the responsivity of our transparent device can reach to 32.5 mA W^{-1} , comparable to those of previously reported examples (Table 1). According to the value of R , two other important figure of merits can be evaluated.^[33,45,46] The corresponding detectivity (D) and the noise equivalent power (NEP) are often described by Equations (3) and (4)

$$D = R / \sqrt{2qJ_d} \quad (3)$$

$$\text{NEP} = I_d / R \sqrt{2q/I_d} \quad (4)$$

where q is electronic charge, J_d is the dark current density, and I_d is the dark current. The detectivity is independent of device area and found to be $\approx 6 \times 10^9$ Jones, comparable to those of previously works.^[33,46] Moreover, the device shows the lowest possible intensity of ≈ 1 pW verified by the noise equivalent power.

In addition, the response time is a crucial parameter of photodetectors, particularly for the applications in motion detection, dynamic imaging, and high-frequency optical communication.^[56] To measure the real response time of the transparent photodetector, a pulse laser (355 nm) was used as the UV light source, and the photogenerated electric signals were recorded in real-time with an oscilloscope. Figure 4c shows the pulse response of the device at 0 V bias. Surprisingly, the rise time (t_r , defined as the time required for output signal changing from 10 to 90% of the peak output value) is found to be 44 ns. The fall time (t_f , defined as the time required for output signal changing from 90 to 10% of the peak output value) is about 1.85 μs . Note that this response speed is among the best performance of self-powered UV photodetectors, as summarized in Table 1. It is well known that the response speed of a photodetector is strongly related to kinetics during transport and collection of photogenerated carriers. Similar to the ZnO/GaN nanoscale p–n junctions reported by Yu and co-workers,^[28] the ultrafast response of our transparent devices is dominated by the drift time of carriers inside the depletion layer of Schottky junction. The charge carriers in the sandwiched structure are separated along the thickness direction, which is consistent with the direction of built-in electric field formed by the Schottky junction. The path length over which charge carriers diffuse is shorter than 200 nm (i.e., the thickness of TiO₂ film, see Figure 1b). Therefore, the sandwich structure makes full use of the local electric field to ensure very efficient and fast collection of the photogenerated carriers. Reducing the film thickness may further increase the response speed, but it concurrently sacrifices light absorption and increases the leakage current. Therefore, a thickness of ≈ 200 nm was chosen in our photodetectors.

Table 1. The performance of the self-powered UV photodetectors.

Photodetector	Wavelength	Responsivity	Rise time	Fall time	Photodark current ratio	Ref.
FTO/TiO ₂ /Ag NWs	350 nm	32.5 mA W ⁻¹	44 ns	1.849 μs	1.7×10^3	This work
TiO ₂ /NiO	350 nm	65 $\mu\text{A W}^{-1}$	1.2 s	7.1 s	14	[47]
n-Ga ₂ O ₃ /n-ZnO	251 nm	9.7 mA W ⁻¹	0.1 ms	0.9 ms	>10 ²	[48]
Pt/GaN/Ni	UV	30 mA W ⁻¹	<0.1 s	<0.1 s	4.67×10^5	[49]
ZnO MSM	365 nm	20 mA W ⁻¹	710 ns	4 μs	–	[50]
Au/ β -Ga ₂ O ₃	254 nm	0.01 mA W ⁻¹	1 μs	60 μs	≈ 15	[51]
ZnO/graphene	380 nm	39 mA W ⁻¹	37 μs	330 μs	–	[52]
SnO ₂ -MS@TiO ₂	365 nm	100 mA W ⁻¹	7 ms	6 ms	1.15×10^5	[53]
TiO ₂ /Ag NWs	350 nm	1.1 mA W ⁻¹	2 ms	47 ms	1.54×10^5	[54]
ZnO/CuCrO ₂	395 nm	5.87 mA W ⁻¹	32 μs	35 μs	–	[55]

Next, we investigated the spectra response of the transparent photodetector. The wavelength dependent response was measured by illuminating the device with a tunable monochromatic light source. Figure 4d shows the spectroscopic photoresponse of our self-powered photodetector to the light of different wavelengths (200–450 nm). It can be seen that the responsivity to an incident light with wavelength greater than 400 nm is rather low, suggesting that the UV photodetector presented here is intrinsically “visible-blind,” which is very attractive in the field of flame sensing, missile guidance systems, and UV communications.^[57] The responsivity gradually increases with the decrease of wavelength and exhibits the maximum at 210 nm. The photoconductive gain (G) is another important parameter, defined as a number of detected carriers per absorbed photon.^[58] It can be calculated by a version of Equation (5)

$$G = R \cdot h \cdot c / (\lambda \cdot q) \quad (5)$$

Here, R is the responsivity, h is the Planck constant, c is the speed of light, λ is the wavelength, and q is electronic charge. The corresponding gain curve is plotted in Figure 4d, showing a similar trend to the responsivity. As we know, UV light is divided into three regions based on its wavelength, namely, UVC (200–280 nm), UVB (280–320 nm), and UVA

(320–400 nm).^[59] Notably, the detection wavelength range of our transparent photodetector can cover the entire UV band. Such a broadband response capability is superior to those reported self-powered UV photodetectors.^[48,51] This is attributed to the absorption of TiO_2 films and the enhanced transparency of Ag NWs electrodes at short wavelengths (see Figure 2c).

Since the device is transparent, omnidirectionality is another potential advantage, as the UV light can illuminate from both sides.^[60] The incident angle-dependent photoresponsivity is an important feature of transparent photodetector. We believe that incident angle dependency is closely related to the symmetry of the device. As shown in Figure 5a, the transparent photodetector is rotationally symmetric in the x - y plane. So the photoresponse will not change with the rotation angle (θ , defined as the angle in the x - y plane at which the device is rotated from its initial position). Figure 5b shows the 360° transient photoresponse under pulsating light, in which the steady-state current remains the same. However, the device is asymmetrical in the thickness direction (z axis). Although the UV light can illuminate from both sides, the generated photoresponse was different from each other. Figure 5c shows the transient photoresponse of one device under 365 nm UV illumination. The photocurrent with the front illumination (from the Ag NWs side) is higher than that with back illumination (from the FTO side). This is because the transmittance of

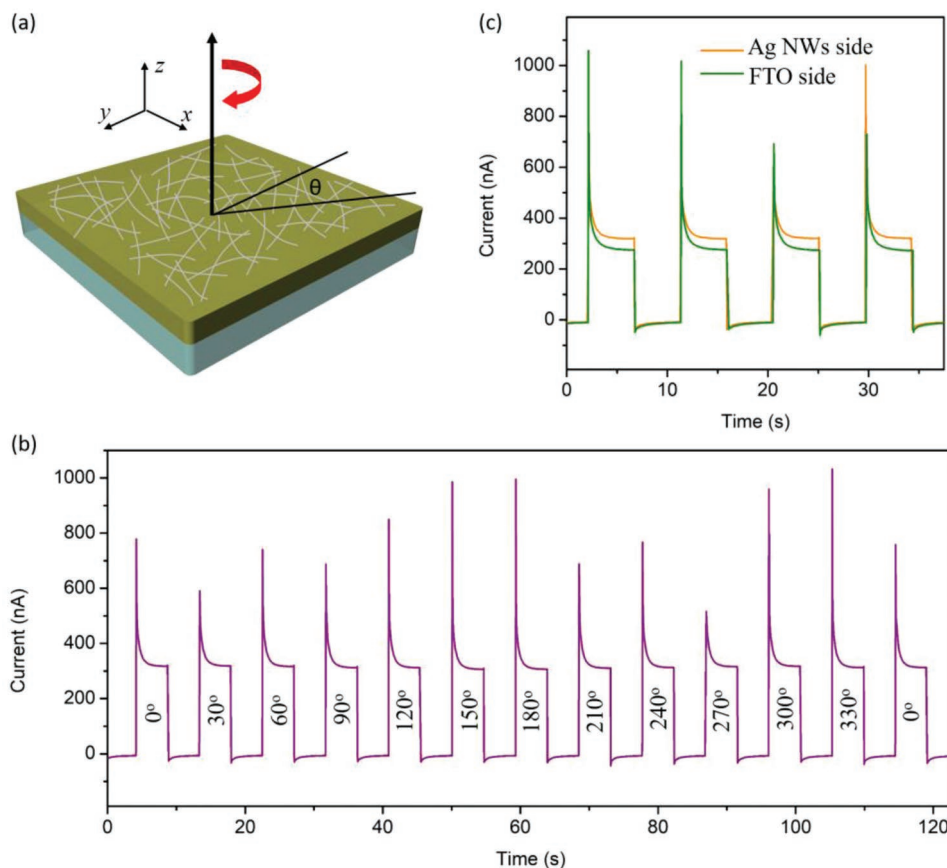


Figure 5. a) An illustration of the rotationally symmetric photodetector. b) The 360° photoswitching behaviors of the transparent photodetector with different rotation angle. c) The transient photoresponse of the transparent photodetector with front and back illumination.

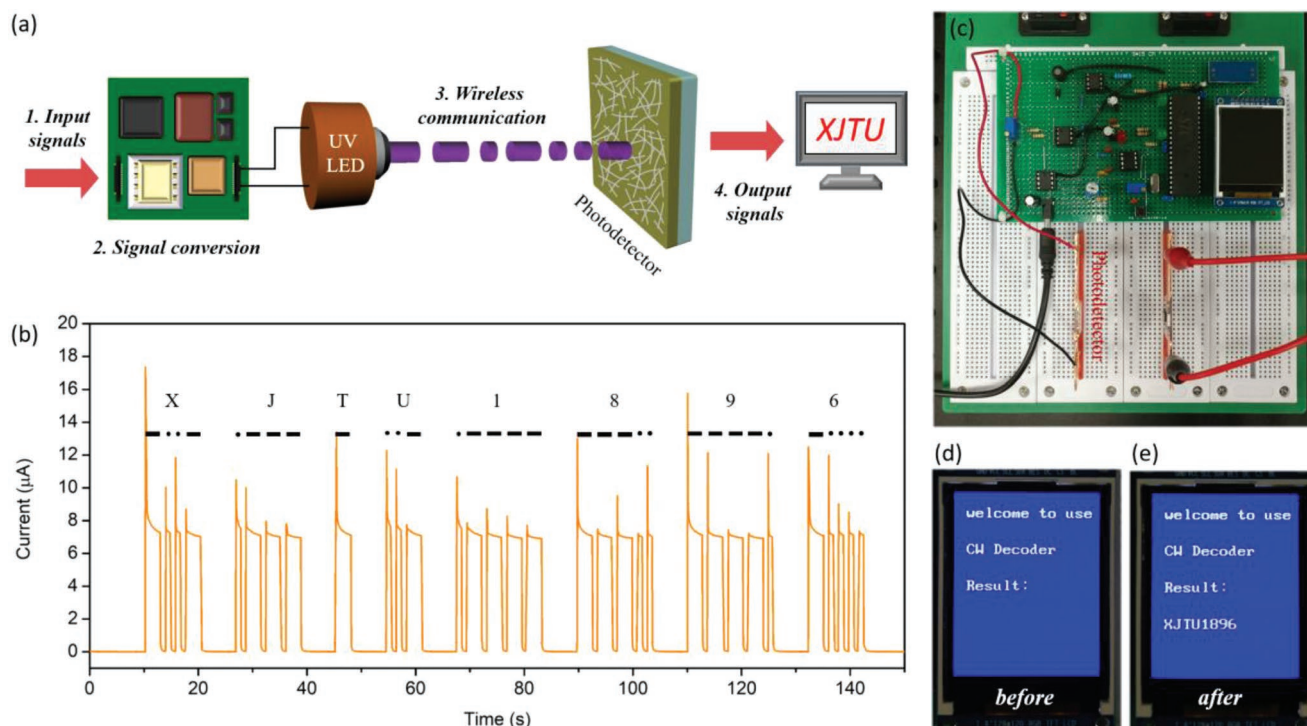


Figure 6. a) Schematic diagram of the UV communication system based on the self-powered UV photodetector. b) Morse code for four letters “XJTU” and four numbers “1896” as the received signals. c) A proof of concept of the UV communication system. d,e) The decoding result before and after receiving signals.

Ag NWs in the UV region is higher than that of FTO electrode. As shown in Figure 2c, FTO glass substrate has a significant absorption in the deep UV range, photons are blocked from reaching the TiO₂ layer. So the photoresponse of UVC can only be obtained from the front illumination. The device has almost no photoresponse to UVC under the back illumination. Such a unique response difference can help us to quickly determine whether the incident light is UVC.

Taking advantage of its high responsivity and ultrafast response speed, we further designed a UV communication system based on our transparent photodetector as a self-powered signal receiver, as shown in Figure 6a. To test the feasibility of alpha-numeric data communication, the input signals “XJTU1896” were first encrypted by international Morse code (details can be found in Figure S4, Supporting Information). After signal conversion, the message was sent by a program-controlled UV light emitting diode (LED) with a center wavelength of 270 nm (the light intensity is $\approx 350 \mu\text{W}$). The UV signals were wirelessly transmitted in free space and recognized by the transparent photodetector. We measured the current signals generated by the photodetector and draw them in Figure 6b. As can be seen from the $I-t$ curve, it shows a sequence of three communication states, namely, dot, dash, and silence. The signal to noise ratio is up to 2000. After decoding these dot and dash sequences, the four characters “XJTU” and four numbers “1896” are then obtained. Figure 6c shows the proof of concept of the UV communication system, in which a decoding module and a color display are used for visualization. The circuit diagram and corresponding decoding mechanism can be found in Figures S5 and S6 (Supporting Information). After

connecting the photodetector to the decoding module, the received UV signals can be converted to text. As shown in Figure 6d,e, the output signals of “XJTU1896” are precisely presented on the color display, which strongly proved the feasibility of the UV communication system. Since the information is compiled by the Morse code, and the information carrier is solar blind UV light (invisible to the human eye), this is a highly confidential way of communication. Along with the features such as high speed, low energy consumption, and anti-electromagnetic interference, the transparent photodetector-based communication system shows great potential in a wide range of applications.

3. Conclusion

In conclusion, a fully transparent UV photodetector based on TiO₂ thin film is fabricated by facile solution-processing method. The optical transmission of the whole device is up to 70% in the visible range. Due to the asymmetric Schottky junctions formed in the sandwiched structure, the device can operate without external power sources. An ultrafast response speed of 44 ns is achieved in the transparent photodetector as a result of efficient separation of photogenerated carriers. As a proof of concept, the UV communication system based on the transparent photodetector has been developed, and its capability of data communication has been well demonstrated. The combination of high optical transparency and self-power ability, as well as excellent device performance metrics, make the Ag NWs/TiO₂/FTO sandwich structure an attractive approach to realizing transparent optoelectronic devices.

4. Experimental Section

Materials Synthesis: TiO₂ precursor was synthesized using a sol–gel method at room temperature. 9 mL ethylene glycol monomethyl ether (AR, Sinopharm Chemical Reagent Co., Ltd.) and 3 mL tetrabutyl titanate (99%, Tianjin Tianli Chemical Reagents Ltd.) were mixed by vigorous stirring. Then, 2 mL acetic anhydride (AR, Sinopharm Chemical Reagent Co., Ltd.) was added drop-wise as stabilizer. The resulting mixture was stirred for 3 h and aged overnight to get a light yellow transparent colloidal suspension, as shown in Figure 1a.

Device Fabrication: The FTO substrates (15 × 15 mm² sheets) were sequentially cleaned in an ultrasonic bath with acetone, ethanol, and deionized water. TiO₂ thin films were deposited by spin-coating the precursor on FTO substrates at a speed of 4000 rpm for 20 s. The film was immediately baked at 350 °C to remove the residual organics. The spin coating and bake treatments were repeated three times to obtain a desired thickness. Finally, the films were annealed at 550 °C with a rapid thermal processor in air. The top electrode was fabricated by directly drop casting Ag NWs dispersion (Nanjing XFNANO Materials Tech Co. Ltd) on the surface of annealed TiO₂ thin films.

Characterization: The TiO₂ film structure was characterized by XRD (X'Pert Pro) with Cu Kα radiation. Raman spectra of the annealed TiO₂ film was recorded by a Raman spectroscopy (LabRAM HR Evolution) with a 532 nm laser. The morphologies of the TiO₂ film and Ag NWs electrodes were observed by SEM (FEI Quanta 250 FEG). TEM images were obtained from a Jeol JEM-2100 Plus microscope. Transmittance of all electrodes and devices were estimated by a UV–VIS–NIR spectrometer (PE Lambda 950). Photoelectric performances were analyzed by a digital sourcemeter (Keithley 2410) and a tunable monochromatic light source (Omni—λbright). Unless otherwise stated, samples were vertically illuminated from the Ag NWs side. The light intensity was adjusted with a NOVA II power meter (OPHIR photonics). The response speed was measured by a home-made transient photoresponse measurement system containing a pulse laser (355 nm). All measurements were performed in air at room temperature.

Supporting Information

Supporting Information is available from the Wiley Online Library or from the author.

Acknowledgements

This work was supported by the National Science Foundation of China (Grant No. 61631166004). H.J.F. thanks the support from National Postdoctoral Program for Innovative Talents (Grant No. BX201700185) and China Postdoctoral Science Foundation Funded Project (Grant No. 2017M620447). H.W. thanks the support from Shenzhen DRC project [2018]1433. Instrument Analysis Center of Xi'an Jiaotong University is acknowledged for the great helps in measurements.

Conflict of Interest

The authors declare no conflict of interest.

Keywords

Schottky junctions, self-powered, transparent electronics, ultrafast, UV photodetectors

Received: December 18, 2018

Revised: January 24, 2019

Published online: February 12, 2019

- [1] J. F. Wager, *Science* **2003**, *300*, 1245.
- [2] F. N. Ishikawa, H.-K. Chang, K. Ryu, P.-C. Chen, A. Badmaev, L. G. D. Arco, G. Z. Shen, C. W. Zhou, *ACS Nano* **2009**, *3*, 73.
- [3] S. Ju, A. Facchetti, Y. Xuan, J. Liu, F. Ishikawa, P. Ye, C. W. Zhou, T. J. Marks, D. B. Janes, *Nat. Nanotechnol.* **2007**, *2*, 378.
- [4] S. Kee, N. Kim, B. Park, B. S. Kim, S. Hong, J.-H. Lee, S. Jeong, A. Kim, S.-Y. Jang, K. Lee, *Adv. Mater.* **2018**, *30*, 1703437.
- [5] D. Mccoul, W. Hu, M. Gao, V. Mehta, Q. Pei, *Adv. Electron. Mater.* **2016**, *2*, 1500407.
- [6] H. Cho, J.-M. Choi, S. Yoo, *Opt. Express* **2011**, *19*, 1113.
- [7] K. Nomura, H. Ohta, K. Ueda, T. Kamiya, M. Hirano, H. Hosono, *Science* **2003**, *300*, 1269.
- [8] X. Y. Liu, Y. Q. Gao, G. W. Yang, *Nanoscale* **2016**, *8*, 4227.
- [9] R. F. Service, *Science* **2018**, *360*, 1386.
- [10] X. Pu, M. Liu, X. Y. Chen, J. M. Sun, C. H. Du, Y. Zhang, J. Y. Zhai, W. G. Hu, Z. L. Wang, *Sci. Adv.* **2017**, *3*, e1700015.
- [11] P. Yang, W. Chang, P. Teng, S. Jeng, S. Lin, P. Chiu, J.-H. He, *Proc. IEEE* **2013**, *101*, 1732.
- [12] W. Y. Kong, G. A. Wu, K. Y. Wang, T. F. Zhang, Y. F. Zou, D. D. Wang, L. B. Luo, *Adv. Mater.* **2016**, *28*, 10725.
- [13] L. Meng, Y. F. Li, B. Yao, Z. H. Ding, G. Yang, R. J. Liu, R. Deng, L. Liu, *J. Appl. Phys.* **2016**, *120*, 235306.
- [14] E. Monroy, F. Omnès, F. Calle, *Semicond. Sci. Technol.* **2003**, *18*, R33.
- [15] D. Han, Y. Liu, K. Zhang, P. Luo, M. Zhang, *Opt. Express* **2012**, *20*, 15833.
- [16] Z. Y. Xu, B. M. Sadler, *IEEE Commun. Mag.* **2008**, *46*, 67.
- [17] W. Tian, T. Y. Zhai, C. Zhang, S.-L. Li, X. Wang, F. Liu, D. Q. Liu, X. K. Cai, K. Tsukagoshi, D. Golberg, Y. Bando, *Adv. Mater.* **2013**, *25*, 4625.
- [18] M. X. Hu, F. Teng, H. Y. Chen, M. M. Jiang, Y. Z. Gu, H. L. Lu, L. F. Hu, X. S. Fang, *Adv. Funct. Mater.* **2017**, *27*, 1704477.
- [19] M. Patel, H.-S. Kim, J. Kim, *Adv. Electron. Mater.* **2015**, *1*, 1500232.
- [20] Z. L. Wang, *Adv. Mater.* **2012**, *24*, 280.
- [21] H. J. Fang, H. Tian, J. Li, Q. Li, J. Y. Dai, T.-L. Ren, G. F. Dong, Q. F. Yan, *Nano Energy* **2016**, *20*, 48.
- [22] S. Park, S. Heo, W. Lee, D. Inoue, Z. Jiang, K. Yu, H. Jinno, D. Hashizume, M. Sekino, T. Yokota, K. Fukuda, K. Tajima, T. Someya, *Nature* **2018**, *561*, 516.
- [23] C. Lin, H. Fu, D. Lien, C. Hsu, J.-H. He, *Nano Energy* **2018**, *51*, 294.
- [24] P. Yang, L. Lin, F. Yi, X. Li, K. Pradel, Y. Zi, C. Wu, J.-H. He, Y. Zhang, Z. L. Wang, *Adv. Mater.* **2015**, *27*, 3817.
- [25] Y. Liu, H. Yao, Y. Chen, *J. Phys. Chem. C* **2011**, *115*, 14988.
- [26] L. X. Su, W. Yang, J. Cai, H. Y. Chen, X. S. Fang, *Small* **2017**, *13*, 1701687.
- [27] P. G. Li, H. Z. Shi, K. Chen, D. Y. Guo, W. Cui, Y. S. Zhi, S. L. Wang, Z. P. Wu, Z. W. Chen, W. H. Tang, *J. Mater. Chem. C* **2017**, *5*, 10562.
- [28] Y. Q. Bie, Z. M. Liao, H. Z. Zhang, G. R. Li, Y. Ye, Y. B. Zhou, J. Xu, Z. X. Qin, L. Dai, D. P. Yu, *Adv. Mater.* **2011**, *23*, 649.
- [29] X. Y. Pan, M.-Q. Yang, X. Fu, N. Zhang, Y.-J. Xu, *Nanoscale* **2013**, *5*, 3601.
- [30] X. D. Li, C. T. Gao, H. G. Duan, B. Lu, X. J. Pan, E. Q. Xie, *Nano Energy* **2012**, *1*, 640.
- [31] Y. R. Xie, L. Wei, G. D. Wei, Q. H. Li, D. Wang, Y. X. Chen, S. S. Yan, G. L. Liu, L. M. Mei, J. Jiao, *Nanoscale Res. Lett.* **2013**, *8*, 188.
- [32] M. N. Tahir, B. Oschmann, D. Buchholz, X. W. Dou, I. Lieberwirth, M. Panthöfer, W. Tremel, R. Zentel, S. Passerini, *Adv. Energy Mater.* **2016**, *6*, 1501489.
- [33] S. Abbas, M. Kumar, H. Kim, J. Kim, J.-H. Lee, *ACS Appl. Mater. Interfaces* **2018**, *10*, 14292.
- [34] N.-G. Park, J. Lagemaat, A. J. Frank, *J. Phys. Chem. B* **2000**, *104*, 8989.
- [35] F. Tian, Y. P. Zhang, J. Zhang, C. X. Pan, *J. Phys. Chem. C* **2012**, *116*, 7515.

- [36] W. F. Zhang, Y. L. He, M. S. Zhang, Z. Yin, Q. Chen, *J. Phys. D: Appl. Phys.* **2000**, *33*, 912.
- [37] P. Görrn, M. Sander, J. Meyer, M. Kröger, E. Becker, H.-H. Johannes, W. Kowalsky, T. Riedl, *Adv. Mater.* **2006**, *18*, 738.
- [38] H. Bao, C. M. Li, X. Cui, Y. Gan, Q. Song, J. Guo, *Small* **2008**, *4*, 1125.
- [39] M. Chen, R. Zha, Z. Yuan, Q. Jing, Z. Huang, X. Yang, S. Yang, X. Zhao, D. Xu, G. Zou, *Chem. Eng. J.* **2017**, *313*, 791.
- [40] J. Kim, C. Kim, Y. Kim, Y. Loo, *Appl. Phys. Lett.* **2009**, *95*, 183301.
- [41] L. Alibabaei, B. D. Sherman, M. R. Norris, M. K. Brennaman, T. J. Meyer, *Proc. Natl. Acad. Sci. USA* **2015**, *112*, 5899.
- [42] J. Q. Liu, L. L. Ruan, S. B. Adeloju, Y. C. Wu, *Dalton Trans.* **2014**, *43*, 1706.
- [43] Y. Wang, T. Sun, X. L. Liu, H. M. Zhang, P. Liu, H. G. Yang, X. D. Yao, H. J. Zhao, *Phys. Rev. B* **2014**, *90*, 045304.
- [44] H. J. Fang, J. W. Li, J. Ding, Y. Sun, Q. Li, J.-L. Sun, L. D. Wang, Q. F. Yan, *ACS Appl. Mater. Interfaces* **2017**, *9*, 10921.
- [45] C. Xie, F. Yan, *Small* **2017**, *13*, 1701822.
- [46] S. Abbas, M. Kumar, J. Kim, *Mater. Sci. Semicond. Process.* **2018**, *88*, 86.
- [47] L. X. Zheng, F. Teng, Z. M. Zhang, B. Zhao, X. S. Fang, *J. Mater. Chem. C* **2016**, *4*, 10032.
- [48] B. Zhao, F. Wang, H. Chen, L. Zheng, L. Su, D. Zhao, X. S. Fang, *Adv. Funct. Mater.* **2017**, *27*, 1700264.
- [49] M. Z. Peng, Y. D. Liu, A. F. Yu, Y. Zhang, C. H. Liu, J. Y. Liu, W. Wu, K. Zhang, X. Q. Shi, J. Z. Kou, J. Y. Zhai, Z. L. Wang, *ACS Nano* **2016**, *10*, 1572.
- [50] H. Y. Chen, K. W. Liu, X. Chen, Z. Z. Zhang, M. M. Fan, M. M. Jiang, X. H. Xie, H. F. Zhao, D. Z. Shen, *J. Mater. Chem. C* **2014**, *2*, 9689.
- [51] X. Chen, K. W. Liu, Z. Z. Zhang, C. R. Wang, B. H. Li, H. F. Zhao, D. X. Zhao, D. Z. Shen, *ACS Appl. Mater. Interfaces* **2016**, *8*, 4185.
- [52] L. Duan, F. N. He, Y. Tian, B. Sun, J. Fan, X. C. Yu, L. Ni, Y. Zhang, Y. N. Chen, W. X. Zhang, *ACS Appl. Mater. Interfaces* **2017**, *9*, 8161.
- [53] Y. W. Huang, Q. J. Yu, J. Z. Wang, X. C. Li, Y. Yan, S. Y. Gao, F. F. Shi, D. B. Wang, C. L. Yu, *Electron. Mater. Lett.* **2015**, *11*, 1059.
- [54] J. Z. Xu, W. Yang, H. Y. Chen, L. X. Zheng, M. X. Hu, Y. M. Li, X. S. Fang, *J. Mater. Chem. C* **2018**, *6*, 3334.
- [55] T. Cossuet, J. Resende, L. Rapenne, O. Chaix-Pluchery, C. Jiménez, G. s Renou, A. J. Pearson, R. L. Z. Hoye, D. Blanc-Pelissier, N. D. Nguyen, E. Appert, D. Muñoz-Rojas, V. Consonni, J.-L. Deschanvres, *Adv. Funct. Mater.* **2018**, *28*, 1803142.
- [56] L. T. Dou, Y. Yang, J. B. You, Z. R. Hong, W.-H. Chang, G. Li, Y. Yang, *Nat. Commun.* **2014**, *5*, 5404.
- [57] N. Nasiri, R. Bo, F. Wang, L. Fu, A. Tricoli, *Adv. Mater.* **2015**, *27*, 4336.
- [58] H. Zhang, A. V. Babichev, G. Jacopin, P. Lavenus, F. H. Julien, A. Y. Egorov, J. Zhang, T. Pauporté, M. Tchernycheva, *J. Appl. Phys.* **2013**, *114*, 234505.
- [59] H. Ju, Y. S. Jiang, B. Xue, Y. J. Xu, H. G. Guo, M. Y. Huo, F. F. Li, *New J. Chem.* **2018**, *42*, 9260.
- [60] D. Lien, H. Wang, S. Chen, Y. Chi, C. Wu, G. Lin, Y. Liao, J.-H. He, *npj. Flex. Elect.* **2018**, *19*.